Optics & Laser Technology 91 (2017) 116–119

Contents lists available at ScienceDirect

Optics & Laser Technology

journal homepage: www.elsevier.com/locate/optlastec

Full length article

# Surface nano-hardness and microstructure of a single crystal nickel base superalloy after laser shock peening

G.X. Lu[a,c], J.D. Liu[a,c,*], H.C. Qiao[b,c], Y.Z. Zhou[a,c], T. Jin[a,c], J.B. Zhao[b,c], X.F. Sun[a,c], Z.Q. Hu[a,c,1]

[a] Institute of Metal Research, Chinese Academy of Sciences, 72 Wenhua Road, Shenyang 110016, China
[b] Shenyang Institute of Automation, Chinese Academy of Sciences, 114 Nanta Road, Shenyang 110016, China
[c] University of Chinese Academy of Sciences, 19 Yuquan Road, Beijing 100049, China

ARTICLE INFO

*Keywords:*
Metals and alloys
Laser processing
Indentation and hardness
Microstructure

ABSTRACT

Nanoindention tests and SEM microstructure observations were conducted on a single crystal nickel base superalloy after laser shock peening (LSP). Distinct surface hardening behavior was found to occur under the selected LSP technology. A large discrepancy in γ′ areas happened on laser shocked regions and the large plastic deformation embodied in γ′ phases' deformation brought a significant hardening effect.

## 1. Introduction

Single crystal nickel base superalloys have been used commonly as blade materials for aircraft turbines because of their good resistance to plastic deformation [1,2]. The microstructure of these alloys consists of a γ matrix in which cuboidal γ′ precipitates are embedded coherently and one of the most striking material characteristics of them is the anisotropy [2]. Laser shock peening (LSP) is used to enhance material lifetimes predominantly under fatigue-related conditions [3–6]. The laser shock effects on mechanical properties of metallic materials, such as steel [7,8], aluminum [9–11], titanium [12–14], have been studied extensively over the last few decades due to the requirement of high fatigue resistance. However, few studies have reported on how the mechanical properties are affected by LSP for single crystal superalloys, particularly in terms of the nano-hardness. This paper describes how the nano-hardnesses are affected by LSP for a single crystal nickel base superalloy. In addition, the corresponding microstructure evolution and deformation mechanism are also involved.

## 2. Experimental

The nominal chemical composition of the selected single crystal nickel base superalloy was listed in Table 1. And the related heat treatment was carried out on the alloy as follows: homogenization (1300 °C/2 h+1310 °C/2 h, air cooling (AC)) and two-step annealing (1130 °C/4 h, AC+900 °C/16 h, AC). The single crystal specimen was cut into rectangular shape with edge length no less than 7 mm. The surfaces peened by LSP were those roughly parallel to [001] orientation and they were mechanically polished prior to the LSP treatment.

The process of LSP was implemented through a Nd:YAG laser operating at 2 Hz with a wavelength of 1064 nm, laser local diameter of 2 mm, laser energy 6 J per pulse and the full wave at half maximum (FWHM) of the pulse of 14 ns. The laser intensity was about 13.6 GW/cm$^2$ under this experimental condition. Before laser irradiation, the sample surface to be processed was coated with a black tape and a flowing water curtain in sequence. The black tape was served as an ablative medium, and the flowing water was used as a confining layer [15,16]. Of particular note is that the sample was treated by one single laser spot with one time.

After the LSP treatment the sample surface was taken to conduct nano-hardness tests. Nanoindention tests were performed using Agilent Nano Indenter G200 equipped with a Berkovich diamond indenter. A load of 13.7 mN, corresponding to an equivalent penetration diameter of ~1.8 μm, was applied for each indent to probe a large volume compared to the γ/γ′ microstructure [17]. The regions with certain distances to the center of laser spot were measured twice. Microstructures of different laser treated regions after chemical etching were analyzed by JEOL JSM-5800 scanning electron microscopy (SEM), which was used at voltage of 20 kV. Moreover, γ′ sizes were quantitated through Image Pro software.

* Corresponding author.
*E-mail addresses:* jdliu@imr.ac.cn (J.D. Liu), tjin@imr.ac.cn (T. Jin).
[1] Deceased.

http://dx.doi.org/10.1016/j.optlastec.2016.12.032
Received 25 July 2016; Received in revised form 28 November 2016; Accepted 27 December 2016

**Table 1**
Nominal chemical composition (wt%) of the selected experimental alloy.

| Co | Cr | W | Al | Mo | Ta | Re | Ni |
|---|---|---|---|---|---|---|---|
| 7–9 | 6–8 | 4–6 | 6–8 | 2–4 | 6–8 | 3–4 | Bal. |

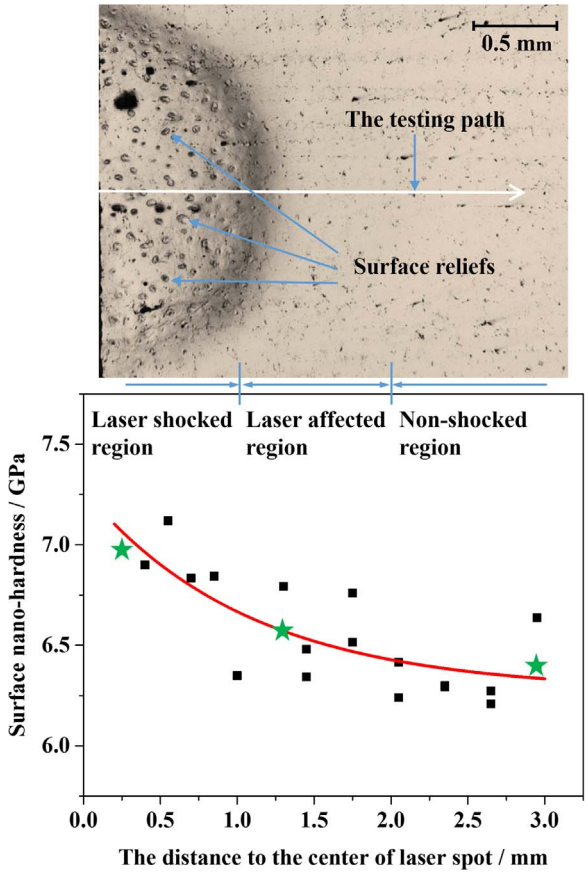


**Fig. 1.** The measured nano-hardness values of different laser treated regions in the indentation test. Above is the metallographic graph of the sample surface after LSP, and the nanoindention testing path was graphically illustrated. The three green stars indicate the testing points in Fig. 2. (For interpretation of the references to color in this figure legend, the reader is referred to the web version of this article.)

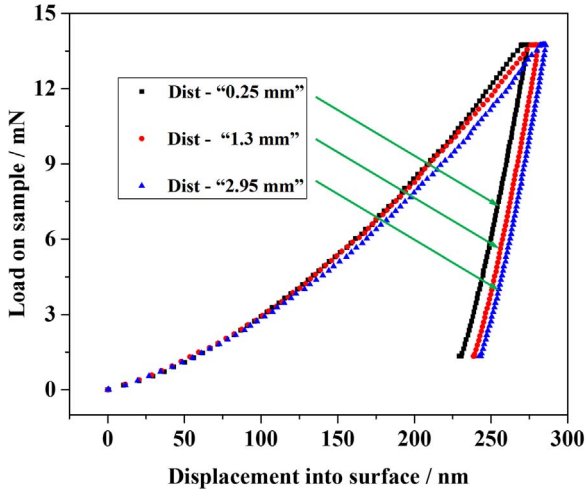


**Fig. 2.** The measured load-displacement curves at a maximum load of about 13.7 mN in the indention test. "Dist-X" represents the testing point which keeps a distance of X to the center of laser spot.

## 3. Results

A circle pit formed on sample surface after laser shock treatment, and a testing path from the center of laser spot to non-shocked regions was chosen as shown in Fig. 1. Three varied laser treated regions could be identified according to the distance to the center of laser spot along the testing path, namely laser shocked regions, laser affected regions and non-shocked regions, respectively. It should be pointed out that, during the nanoindention tests, the surface relief zones [18] on the laser shocked regions were avoided for reducing errors.

Hardness cartography was established to map out the local surface hardness of different laser treated regions in Fig. 1. By means of abnormal data deletion, the known nano-hardness data were fitted with an exponent to form a curve. The nanoindention results of Fig. 1 presented the significant hardening effect for the laser shocked regions. And it can be gained that the hardnesses of the three regions was on the decrease. Fig. 2 was constructed to demonstrate detailed load-displacement curves of the labelled testing points in Fig. 1 additionally. It showed a diversity in penetration depths of the three testing points under the same indention load and the varied penetration depths corresponded to the different nano-hardness kept. Namely that the testing point, which kept a larger hardness, obtained a relatively small penetration depth.

A detailed analysis of the microstructure in different laser treated regions was performed using SEM images of the surface. The observation zones with distances to the center of laser spot of about 0.6 mm, 1.2 mm and 2 mm were selected and the corresponding SEM graphs were shown in Fig. 3. It was observed from Fig. 3(a, b) that the γ′ cubes' edges were not well aligned, attesting to a scatter in the size of the γ′ precipitates. In contrast, Fig. 3(c) gained a relative uniformity in the sizes of the γ′ precipitates. As for γ channels, a distinct change was gained that the widths of γ channels in Fig. 3(a) became inhomogeneous. Some widened and narrowed γ channels appeared in Fig. 3(a) as compared to the origin γ channels shown in Fig. 3(c).

## 4. Discussions

Laser shock achieves its reinforcement effect via surface severe plastic deformation [19]. Large nano-hardnesses kept by laser shocked regions are due to the high work hardening level generated by large plastic deformation degree [4]. The specific manifestations of the large deformation are expressed detailedly as follows.

The sizes of γ′ precipitates were characterized through areas. The values of γ′ areas were estimated from Fig. 3 by using Image Pro software and statistic data of γ′ areas were used to establish the associated probability density function (PDF) (Fig. 4). In terms of the PDF of γ′ areas shown in Fig. 4, γ′ areas showed a greater dispersion degree for the laser shocked and affected regions as compared to the sizes of γ′ precipitates in non-shocked regions. Further, the average areas of γ′ precipitates of the two laser treated regions slightly increased. The statistical data of γ′ precipitates were listed in Table 2 and different distortion degrees of γ′ precipitates for different regions were confirmed by quantitative assessments.

Some experimental results of previous publications confirm that, as the main strengthening phase, γ′ precipitates possess the higher strength and hardness than γ matrix phases [17,20]. And therefore γ′ precipitates are of a relatively strong resistance to deformation. Extrusion deformation generally happens on material surface under the impact of high pressure. Under the given condition, the γ′ precipitates deform in the mode of lateral expansion (Parallel to sample surface), and therefore γ channels are directly extruded. On the basis of the principle of volume invariably, γ channels extend longitudinally (The opposite direction of laser shock) simultaneously. Schematic diagrams of longitudinal section were given in Fig. 3 and it illustrated the mentioned deformation mechanism. Given that, the lateral expansion of γ′ precipitates resulted in the larger γ′ area in

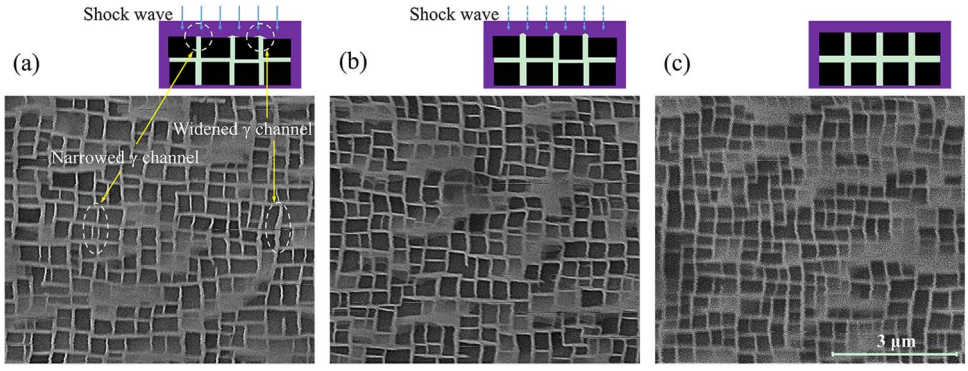


**Fig. 3.** The SEM micrographs of sample surfaces with varied distances to the center of laser spot. (a), (b), (c) represent the laser-shocked region, laser-affected region and non-shocked region respectively.

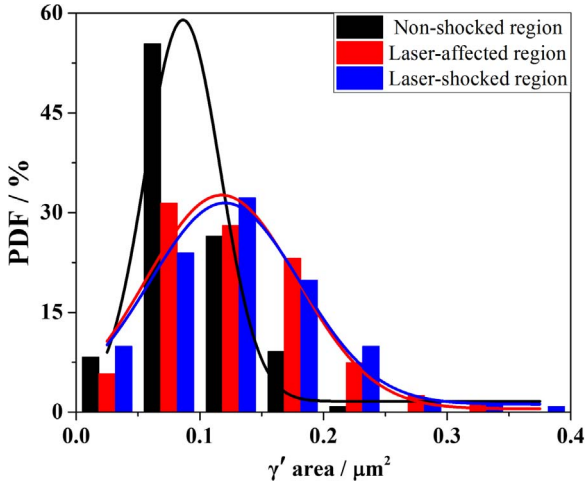


**Fig. 4.** Statistical data (Histogram) and associated probability density function (PDF) of γ′ area in different laser treated regions.

**Table 2**
Average area of γ′ phase and standard deviation of γ′ areas for different regions.

| Regions | Average area of γ′ phase/ μm² | Standard deviation of γ′ areas |
|---|---|---|
| Laser-shocked region | 0.132 | 0.064 |
| Laser-affected region | 0.127 | 0.062 |
| Non-shocked region | 0.095 | 0.036 |

Fig. 3(a, b). And the inhomogeneity of deformation in γ′ precipitates and γ channels gave rise to the larger standard deviation of γ′ areas.

A striking phenomenon was found that the size of γ channel was also changeable due to laser shock. As identified in Fig. 3(a) with arrows, the width of γ channel diverged. The formation of the narrowed γ channels could be ascribed to the squeezing action of the nearby γ′ phases as previously noted. From the schematic diagrams of longitudinal section given in Fig. 3(a, b), the formation mechanism of the widened γ channels was easily gained. Under the effect of laser shock, the lateral expansion of γ′ precipitates promoted the longitudinal plastic flow of γ channels and as a result that γ channels protruded from the plain surface. A convex shape kept by γ channels was presented in Fig. 3(b). When the prominent part of γ channel was small, impact load limited its plastic flow inside the material. Nevertheless, for another case, the prominent part of γ channel was so big that impact load could not restrict its plastic flow inside the material completely. The prominent part was squashed on sample surface and the appeared widened γ channels formed in this way.

## 5. Conclusion

Nano-hardness tests and microstructure observations were conducted on different laser treated regions. The nano-hardnesses of the laser shocked regions increased dramatically. In addition, for the laser shocked regions, both γ′ size and standard deviation of γ′ sizes were larger as compared to the origin surface regions. The γ′ deformation indicated that a large deformation degree was obtained by the laser shocked regions and the brilliant hardening effect resulted from that.

## Acknowledgements

This work is partly supported by the High Technology Research and Development Program of China (No. 2014AA041701), the National Natural Science Foundation of China (Nos. 51171179, 51271174, 51331005, 51501219, and 11332010) and the Natural Science Foundation of Liaoning Province in China (No. 2015020115).

## References

[1] P. Lukáš, J. Čadek, V. Šustek, L. Kunz, Creep of CMSX-4 single crystals of different orientations in tension and compression, Mater. Sci. Eng.: A 208 (1996) 149–157.
[2] R.C. Reed, The Superalloys: Fundamentals and Applications, Cambridge University Press, New York, 2006.
[3] P. Peyre, R. Fabbro, P. Merrien, H.P. Lieurade, Laser shock processing of aluminium alloys. application to high cycle fatigue behaviour, Mater. Sci. Eng. A-Struct. Mater. Prop. Microstruct. Process. 210 (1996) 102–113.
[4] R. Fabbro, P. Peyre, L. Berthe, X. Scherpereel, Physics and applications of laser-shock processing, J. Laser Appl. 10 (1998) 265–279.
[5] Y. Li, L. Zhou, W. He, G. He, X. Wang, X. Nie, B. Wang, S. Luo, Y. Li, The strengthening mechanism of a nickel-based alloy after laser shock processing at high temperatures, Sci. Technol. Adv. Mater. 14 (2013) 1574–1578.
[6] Y. Liao, S. Suslov, C. Ye, G.J. Cheng, The mechanisms of thermal engineered laser shock peening for enhanced fatigue performance, Acta Mater. 60 (2012) 4997–5009.
[7] M. Gerland, M. Hallouin, Effect of pressure on the microstructure of an austenitic stainless steel shock-loaded by very short laser pulses, J. Mater. Sci. 29 (1994) 345–351.
[8] S. Kalainathan, S. Sathyajith, S. Swaroop, Effect of laser shot peening without coating on the surface properties and corrosion behavior of 316L steel, Opt. Lasers Eng. 50 (2012) 1740–1745.
[9] X.D. Ren, L. Ruan, S.Q. Yuan, H.M. Yang, Q.B. Zhan, L.M. Zheng, Y. Wang, F.Z. Dai, Metallographic structure evolution of 6061-T651 aluminum alloy processed by laser shock peening: effect of tempering at the elevated temperatures, Surf. Coat. Technol. 221 (2013) 111–117.
[10] B. Rouleau, P. Peyre, J. Breuils, H. Pelletier, T. Baudin, F. Brisset, Characterization at a local scale of a laser-shock peened aluminum alloy surface, Appl. Surf. Sci. 257 (2011) 7195–7203.
[11] C. Correa, D. Peral, J.A. Porro, M. Díaz, L. Ruiz de Lara, A. García-Beltrán, J.L. Ocaña, Random-type scanning patterns in laser shock peening without absorbing coating in 2024-T351 Al alloy: a solution to reduce residual stress anisotropy, Opt. Laser Technol. 73 (2015) 179–187.
[12] W. Jia, Q. Hong, H. Zhao, L. Li, D. Han, Effect of laser shock peening on the mechanical properties of a near-α titanium alloy, Mater. Sci. Eng.: A 606 (2014) 354–359.
[13] R.K. Nalla, I. Altenberger, U. Noster, G.Y. Liu, B. Scholtes, R.O. Ritchie, On the influence of mechanical surface treatments—deep rolling and laser shock peening—on the fatigue behavior of Ti–6Al–4V at ambient and elevated temperatures, Mater.

Sci. Eng.: A 355 (2003) 216–230.
[14] X.C. Zhang, Y.K. Zhang, J.Z. Lu, F.Z. Xuan, Z.D. Wang, S.T. Tu, Improvement of fatigue life of Ti-6Al-4V alloy by laser shock peening, Mater. Sci. Eng. A-Struct. Mater. Prop. Microstruct. Process. 527 (2010) 3411–3415.
[15] X.Q. Zhang, H. Li, X.L. Yu, Y. Zhou, S.W. Duan, S.Z. Li, Z.L. Huang, L.S. Zuo, Investigation on effect of laser shock processing on fatigue crack initiation and its growth in aluminum alloy plate, Mater. Des. 65 (2015) 425–431.
[16] G.X. Lu, J.D. Liu, H.C. Qiao, G.L. Zhang, C.Y. Cui, Y.Z. Zhou, T. Jin, J.B. Zhao, X.F. Sun, Z.Q. Hu, Microscopic surface topography of a wrought superalloy processed by laser shock peening, Vacuum 130 (2016) 25–33.
[17] C. Tromas, M. Arnoux, X. Milhet, Hardness cartography to increase the nanoindentation resolution in heterogeneous materials: application to a Ni-based single-crystal superalloy, Scr. Mater. 66 (2012) 77–80.
[18] G.X. Lu, J.D. Liu, H.C. Qiao, Y.Z. Zhou, T. Jin, X.F. Sun, Z.Q. Hu, Nonuniformity of morphology and mechanical properties on the surface of single crystal superalloy subjected to laser shock peening, J. Alloy. Compd. 658 (2016) 721–725.
[19] S. Srinivasan, D.B. Garcia, M.C. Gean, H. Murthy, T.N. Farris, Fretting fatigue of laser shock peened Ti–6Al–4V, Tribol. Int. 42 (2009) 1324–1329.
[20] D. Lee, An investigation of thermal aging effects on the mechanical properties of a Ni3Al-based alloy by nanoindentation, J. Alloy. Compd. 480 (2009) 347–350.